CHAPTER V

STUDIES OF SO_2 AND O_2 INDUCED DEGRADATION OF AQUEOUS MEA SOLUTION DURING CO_2 ABSORPTION FROM POWER PLANT FLUE GAS STREAMS

5.1 Research Objectives

One of the major disadvantages of using MEA is its high energy requirement for CO_2 regeneration relative to DEA and MDEA (Veawab et al., 2003). The other major setback is that MEA has a limitation that its maximum CO_2 loading capacity based on stoichiometry is about 0.5 mol CO_2/mol amine unlike tertiary amines such as MDEA, which have an equilibrium CO_2 loading capacity that approaches 1 mol CO_2/mol amine. Furthermore, MEA undergoes degradation when exposed to coal fired power plant flue gas composed of CO_2, fly ash, O_2, N_2, SO_2 and NO_2 (Bello and Idem, 2005; 2006; Idem, et al., 2006). Fly ash is the fine particulates in flue gas consisting of inorganic oxides such as SiO_2, Al_2O_3, Fe_2O_3, CaO, MgO, Na_2O, K_2O and P_2O_5. This alkanolamine breakdown deteriorates the performance of the alkanolamine in the absorption process. Not only does it reduce the CO_2 removal capacity, but also, corrosion and foaming are induced due to the presence of degradation products (Rooney, Bacon, and Dupart, 1996; Rooney, Dupart, and Bacon, 1997). The prediction of the extent and rate of alkanolamine degradation is vital in the estimation of the exact alkanolamine make-up rate needed to maintain the CO_2 absorption capacity of the capture process. It is also essential to evaluate the kinetics of the degradation process since this provides the elements for a better understanding of the degradation mechanism during the CO_2 absorption operation. A kinetic evaluation also helps in the formulation of a degradation prevention strategy which is considered to be the overall goal of degradation studies (Rochelle et al., 2002).

The present study was conducted to establish the roles of the degradation species and to achieve a more realistic scenario as used in CO_2 absorption from both coal- and natural gas-fired power plant flue gas streams. This was based on

developing mechanism based kinetic models for degradation of MEA in the presence of aqueous MEA, O_2, SO_2 and CO_2.

5.2 Theory

All kinetic models were formulated based on the assumption that MEA reacted only in the liquid phase with dissolved O_2, SO_2 and CO_2. Such an assumption is justified based on previous experience (Supap et al., 2001) in which under similar experimental conditions, the vapor pressure of the system before introduction of the simulated gaseous reactants was mostly due to water vapor. This enabled elimination of MEA vapor and thus eliminates any gas phase reaction. This allowed the degradation kinetics to be formulated as a homogeneous liquid phase system. Also, as demonstrated in that work (Supap et al., 2001), mass transfer limitations and the interference from degradation products can also be neglected since only the initial rates of MEA degradation are considered. These assumptions together with those of a previous work (Uyanga and Idem, 2007) were used to formulate the kinetic models outlined below.

5.2.1 Power Law Model

A simple power law rate analysis was first used to develop a kinetic model of MEA degradation. The reaction orders with respect to MEA, O_2, SO_2 and CO_2 were assigned as the corresponding stoichiometric coefficients in the reaction as given in Equation (5.1).

$$aMEA + bO_2 + cSO_2 + dCO_2 \rightarrow products \tag{5.1}$$

The corresponding power-law rate equation is as given in Equation (5.2);

$$-r_{MEA} = k[MEA]^a[O_2]^b[SO_2]^c[CO_2]^d \tag{5.2}$$

The temperature dependency of the rate constant (k) was also taken into account as expressed by the well-known Arrhenius equation. Thus, the overall

equation that represents the power law kinetic model of MEA degradation as a function of temperature and the concentrations of MEA, O_2, SO_2 and CO_2 is given in Equation (5.3).

$$-r_{MEA} = k_0 e^{\frac{-E_a}{RT}} [MEA]^a [O_2]^b [SO_2]^c [CO_2]^d \tag{5.3}$$

where $-r_{MEA}$ is the degradation rate of MEA (kmol/m^3.h), k_0 is the preexponential constant (unit depends on the values of a, b, c, and d), E_a is the activation energy (J/mol), R is the gas constant (8.314 J/mol.K), T is the degradation temperature (K), $[MEA]$, $[O_2]$, $[SO_2]$, and $[CO_2]$ are respectively MEA, O_2, SO_2, and CO_2 concentrations (kmol/m^3), and a, b, c and d are the respective reaction orders with respect to MEA, O_2, SO_2 and CO_2.

5.2.2 Modified Power Law Model

The use of the kinetic model of Equation (4.3) previously developed is only restricted to the case in which O_2 and SO_2 must be both present in the gas streams. In the case where SO_2 concentration in the gas stream is negligible or essentially zero (e.g. natural gas-fired power plant flue gas), or O_2 concentration in the liquid phase is negligible (e.g. in the stripping column of the CO_2 capture plant), estimation of MEA degradation rate using Equation (5.3) is not appropriate. Consequently, a modification of Equation (5.3) is necessary in order to circumvent this anomaly. This modification is similar to the approach taken in a previous work (Uyanga and Idem, 2007). The modified power law model is presented in Equation (5.4).

$$-r_{MEA} = k_0 e^{\frac{-E_a}{RT}} [MEA]^a ([O_2]^b + [SO_2]^c)[CO_2]^d \tag{5.4}$$

5.2.3 Mechanistic-Based Split Model

In this model, the degradation of MEA in the presence of O_2, SO_2 and CO_2 was thought to occur following two different pathways. The first case was the O_2 pathway representing the degradation of MEA solely induced by O_2 while the second case was the SO_2 pathway entirely responsible for the degradation of MEA induced by SO_2. These two pathways were constructed to represent each case, and mechanistic models were derived based on each pathway. These kinetic equations were subsequently combined to represent the overall mechanistic rate model for both O_2 and SO_2 induced MEA degradation.

5.2.3.1 O_2 Pathway

Mechanistic steps were given based on a modification of a previous kinetic work (Bello and Idem, 2006). The simplified MEA degradation steps are given as follows;

$$aMEA + bO_2 \xrightarrow{k_1} I_1 \tag{5.5}$$

$$I_1 \xrightarrow{k2} products + I_2 \tag{5.6}$$

$$I_2 \xrightarrow{k_3} products \tag{5.7}$$

$$I_2 + eO_2 \xrightarrow{k_4} products \tag{5.8}$$

$$I_2 + fMEA \xrightarrow{k_5} products \tag{5.9}$$

$$I_1 + dCO_2 \xrightarrow{k_6} products \tag{5.10}$$

$$I_2 + gCO_2 \xrightarrow{k_7} products \tag{5.11}$$

$$hMEA + iCO_2 \xrightarrow{k_8} I_3 \tag{5.12}$$

$$I_3 \xrightarrow{k_9} products \tag{5.13}$$

The degradation mechanism consists of nine elementary reaction steps initiated by the reaction of MEA and O_2 to produce the first intermediate (I_1) as shown in Equation (5.5). I_1 further decomposes to form products and the second intermediate (I_2) in Equation (5.6). I_2 could either convert to products in Equation (5.7) or react further with O_2 or MEA respectively represented

by Equations (5.8) and (5.9). Both intermediates, I_1 and I_2, could also react with CO_2 as given in Equations (5.10) and (5.11), respectively. Equation (5.12) shows the interaction between MEA and CO_2 to form the intermediate I_3 followed by its conversion to products as given in Equation (5.13). The overall rate of degradation of MEA derived from these reaction steps is given in Equation (5.14).

$$-r_{MEA} = k_2[I_1] + k_3[I_2] + k_4[I_2][O_2]^e + k_5[I_2][MEA]^f + k_6[I_1][CO_2]^d + k_7[I_2][CO_2]^g + k_9[I_3] \quad (5.14)$$

Equation (5.14) can be rearranged to give Equation (5.15).

$$-r_{MEA} = (k_2 + k_6[CO_2]^d)[I_1] + (k_3 + k_4[O_2]^e + k_5[MEA]^f + k_7[CO_2]^g)[I_2] + k_9[I_3] \quad (5.15)$$

The quantification of intermediates (e.g. I_1, I_2, and I_3) is extremely difficulty. Thus, I_1, I_2 and I_3 were eliminated by substituting measurable species such as MEA, O_2 and CO_2 using the pseudo steady state approximation (Lenvenspiel, 1999) as shown in Equations (5.16), (5.17) and (5.18), respectively.

$$r_{I_1(net)} = 0 = k_1[MEA]^a[O_2]^b - k_2[I_1] - k_6[I_1][CO_2]^d \quad (5.16)$$

$$r_{I_2(net)} = 0 = k_2[I_1] - k_3[I_2] - k_4[I_2][O_2]^e - k_5[I_2][MEA]^f - k_7[CO_2]^g \quad (5.17)$$

$$r_{I_3(net)} = 0 = k_8[MEA]^h[CO_2]^i - k_9[I_3] \quad (5.18)$$

Equations (5.16), (5.17) and (5.18) were rearranged to give Equations (5.19), (5.20) and (5.21), respectively.

$$[I_1] = \frac{k_1[MEA]^a[O_2]^b}{k_2 + k_6[CO_2]^d} \quad (5.19)$$

$$[I_2] = \frac{k_2[I_1]}{k_3 + k_4[O_2]^e + k_5[MEA]^f + k_7[CO_2]^g} \quad (5.20)$$

$$[I_3] = \frac{k_8[MEA]^h[CO_2]^i}{k_9} \tag{5.21}$$

Equation (5.19) was substituted into Equation (5.20) to yield Equation (5.22).

$$[I_2] = \frac{k_1 k_2[MEA]^a[O_2]^b}{(k_2 + k_6[CO_2]^d)(k_3 + k_4[O_2]^e + k_5[MEA]^f + k_7[CO_2]^g)} \tag{5.22}$$

The substitution of Equations (5.19), (5.21) and (5.22) into Equation (5.15) gives Equation (5.23).

$$-r_{MEA} = k_1[MEA]^a[O_2]^b + \frac{k_1 k_2[MEA]^a[O_2]^b}{k_2 + k_6[CO_2]^d} + k_8[MEA]^h[CO_2]^i \tag{5.23}$$

Equation (4.23) is then rearranged to give Equation (5.24).

$$-r_{MEA} = \frac{2k_1 k_2[MEA]^a[O_2]^b + k_1 k_6[MEA]^a[O_2]^b[CO_2]^d}{k_2 + k_6[CO_2]^d} + k_8[MEA]^h[CO_2]^i \tag{4.24}$$

Degradation experiments conducted at 393 K using 5 kmol/m^3 MEA and 100% O_2 with 0.55 mole CO_2 per mole MEA/without CO_2 were used to show the inhibition effect of CO_2. The MEA degradation rate of this run with CO_2 was found to be 0.0084 kmol/m^3.h. This was approximately 2 times slower than that for the run without CO_2 (i.e. 0.0184 kmol/m^3.h) implying that the last term in Equation (5.24) could be neglected. This allowed us to simplify Equation (5.24) by dropping the terms involving the slow degradation reaction of MEA with CO_2, as shown in Equation (5.25).

$$-r_{MEA} = \frac{k[MEA]^a[O_2]^b}{1 + k_1'[CO_2]^d} \tag{5.25}$$

where $k = \frac{2k_1k_2}{k_2}$ and $k_1^{'} = \frac{k_6}{k_2}$

The introduction of the Arrhenius equation to account for the temperature dependency of the rate constant gives the final rate expression of MEA degradation for the O_2 pathway as shown in Equation (5.26).

$$-r_{MEA} = \frac{k_{01}e^{\frac{-E_{a1}}{RT}}[MEA]^a[O_2]^b}{1+k_1^{'}[CO_2]^d} \tag{5.26}$$

5.2.3.2. SO_2 pathway

Degradation steps in SO_2 pathway were thought to be analogous to those of the O_2 route. The steps are given below.

$$a^{'}MEA + cSO_2 \xrightarrow{k_{10}} I_4 \tag{5.27}$$

$$I_4 \xrightarrow{k_{11}} products + I_5 \tag{5.28}$$

$$I_5 \xrightarrow{k_{12}} products \tag{5.29}$$

$$I_5 + mSO_2 \xrightarrow{k_{13}} products \tag{5.30}$$

$$I_5 + nMEA \xrightarrow{k_{14}} products \tag{5.31}$$

$$I_4 + d^{'}CO_2 \xrightarrow{k_{15}} products \tag{5.32}$$

$$I_5 + qCO_2 \xrightarrow{k_{16}} products \tag{5.33}$$

$$sMEA + tCO_2 \xrightarrow{k_{17}} I_6 \tag{5.34}$$

$$I_6 \xrightarrow{k_{18}} products \tag{5.35}$$

A similar approach as for the O_2 pathway was adopted for the derivation of the kinetic model for the SO_2 route as given in Equation (5.36).

$$\begin{aligned} -r_{MEA} &= (k_{11} + k_{15}[CO_2]^{d^{'}})[I_4] + \\ &(k_{12} + k_{13}[SO_2]^m + k_{14}[MEA]^n + k_{16}[CO_2]^q)[I_5] + k_{18}[I_6] \end{aligned} \tag{5.36}$$

Expressions for I_4, I_5 and I_6 are given in Equations (5.37) – (5.39), respectively.

$$[I_4] = \frac{k_{10}[MEA]^{a'}[SO_2]^c}{k_{11} + k_{15}[CO_2]^{d'}} \tag{5.37}$$

$$[I_5] = \frac{k_{10}k_{11}[MEA]^{a'}[SO_2]^c}{(k_{11} + k_{15}[CO_2]^{d'})(k_{12} + k_{13}[SO_2]^m + k_{14}[MEA]^n + k_{16}[CO_2]^q)} \tag{5.38}$$

$$[I_6] = \frac{k_{17}[MEA]^s[CO_2]^t}{k_{18}} \tag{5.39}$$

The substitution of Equations (5.37) - (5.39) into Equation (5.36), rearrangement, neglecting CO_2 reaction terms, and the introduction of the Arrhenius equation give the final rate expression for MEA degradation by SO_2 route shown in Equation (5.40).

$$-r_{MEA} = \frac{k_{02}e^{\frac{-E_{a2}}{RT}}[MEA]^{a'}[SO_2]^c}{1 + k_2'[CO_2]^{d'}} \tag{5.40}$$

where $k_2' = \frac{k_{15}}{k_{11}}$

A direct combination of the rates for the O_2 and SO_2 pathway gives the final overall mechanistic rate model for MEA degradation as shown in Equation (5.41).

$$-r_{MEA} = \frac{k_{01}e^{\frac{-E_{a1}}{RT}}[MEA]^a[O_2]^b}{1 + k_1'[CO_2]^d} + \frac{k_{02}e^{\frac{-E_{a2}}{RT}}[MEA]^{a'}[SO_2]^c}{1 + k_2'[CO_2]^{d'}} \tag{5.41}$$

where k_{01} and k_{02} are the preexponential constants, E_{a1} and E_{a2} are the activation energies (J/mol), k_1' and k_2' are constants and a, b, and d are the respective reaction orders with respect to MEA, O_2, and CO_2 derived from the O_2 pathway, and a', c, and d' are SO_2 pathway-derived reaction orders of MEA, SO_2 and CO_2.

5.2.4 Mechanistic Based-Combined Model

The split model shown in Equation (5.41) was obtained based on the assumption that O_2 and SO_2 independently degraded MEA via separate pathways. The model did not take into account the possible interaction effect of O_2 and SO_2 in degrading MEA which could possibly exist in the degradation system. Therefore, it was decided to also incorporate this effect into the kinetic equation by initially proposing O_2 and SO_2 as a co-contributor in producing a combined intermediate by reacting with MEA. This is represented by Equation (5.42). The rest of the degradation steps were quickly set off following this first step and proceeded likewise as previously derived for O_2 or SO_2 pathways. Based on the SO_2 pathway, modification of mechanism done to incorporate the O_2-SO_2 interaction effect is shown below.

$$\left.\begin{array}{l} aMEA + bO_2 \rightarrow I_1' \\ aMEA + cSO_2 \rightarrow I_2' \end{array}\right\} \succ \xrightarrow{k_{10}} I_4 \qquad (5.42)$$

$$I_4 \xrightarrow{k_{11}} products + I_5 \qquad (5.43)$$

$$I_5 \xrightarrow{k_{12}} products \qquad (5.44)$$

$$I_5 + mSO_2 \xrightarrow{k_{13}} products \qquad (5.45)$$

$$I_5 + nMEA \xrightarrow{k_{14}} products \qquad (5.46)$$

$$I_5 + eO_2 \xrightarrow{k_{15}} products \qquad (5.47)$$

$$I_4 + dCO_2 \xrightarrow{k_{16}} products \qquad (5.48)$$

$$I_5 + qCO_2 \xrightarrow{k_{17}} products \qquad (5.49)$$

$$sMEA + tCO_2 \xrightarrow{k_{18}} I_6 \qquad (5.50)$$

$$I_6 \xrightarrow{k_{19}} products \qquad (5.51)$$

Once again, a similar approach previously used to obtain the rate expressions for O_2 and SO_2 pathways was employed. Thus, the rate of MEA degradation can be expressed in Equation (5.52).

$$-r_{MEA} = (k_{11} + k_{16}[CO_2]^d)[I_4] + (k_{12} + k_{13}[SO_2]^m + k_{14}[MEA]^n + k_{15}[O_2]^e + k_{17}[CO_2]^q)[I_5] + k_{19}[I_6] \quad (5.52)$$

The intermediates I_4, I_5 and I_6 are then modified to give Equations (5.53) – (5.55), respectively.

$$[I_4] = \frac{k_{10}[MEA]^a([O_2]^b + [SO_2]^c)}{k_{11} + k_{16}[CO_2]^d} \quad (5.53)$$

$$[I_5] = \frac{k_{10}k_{11}[MEA]^a([O_2]^b + [SO_2]^c)}{(k_{11} + k_{16}[CO_2]^d)(k_{12} + k_{13}[SO_2]^m + k_{14}[MEA]^n + k_{15}[O_2]^e + k_{17}[CO_2]^q)} \quad (5.54)$$

$$[I_6] = \frac{k_{18}[MEA]^s[CO_2]^t}{k_{19}} \quad (5.55)$$

The final rate expression was finally obtained by substituting Equations (5.53) - (5.55) into Equation (5.52), rearranging, dropping the slow reaction terms involving MEA and CO_2, and then introducing the Arrhenius equation. The combined model is finally given in Equation (5.56).

$$-r_{MEA} = \frac{k_0 e^{\frac{-E_a}{RT}}[MEA]^a([O_2]^b + [SO_2]^c)}{1 + k_2'[CO_2]^d} \quad (5.56)$$

Where k_0 is the preexponential constant, E_a is the activation energy (J/mol), k_2' is the rate constant and a, b, c and d are the respective reaction orders with respect to MEA, O_2, SO_2 and CO_2.

5.3 Results and Discussion

5.3.1 Evaluation of the Roles of Temperature and the Concentrations of MEA, O_2, SO_2 and CO_2

Studies were conducted to evaluate the effects of temperature and the concentrations of MEA, O_2, SO_2 and CO_2 on MEA degradation. The effect of temperature using 5 kmol/m^3 MEA and 100% O_2 is shown in Figure 5.1. It is clear that the degradation rate of the run conducted at 393 K proceeded at a faster rate that those carried out at lower temperatures of 373 and 328 K. MEA degradation rate of 393 K run was respectively about 1.4 and almost 100 times higher than those of runs at 373 K and 328 K. The degradation rate of MEA was also found to increase if temperature increased using the degradation system of MEA-O_2-SO_2.

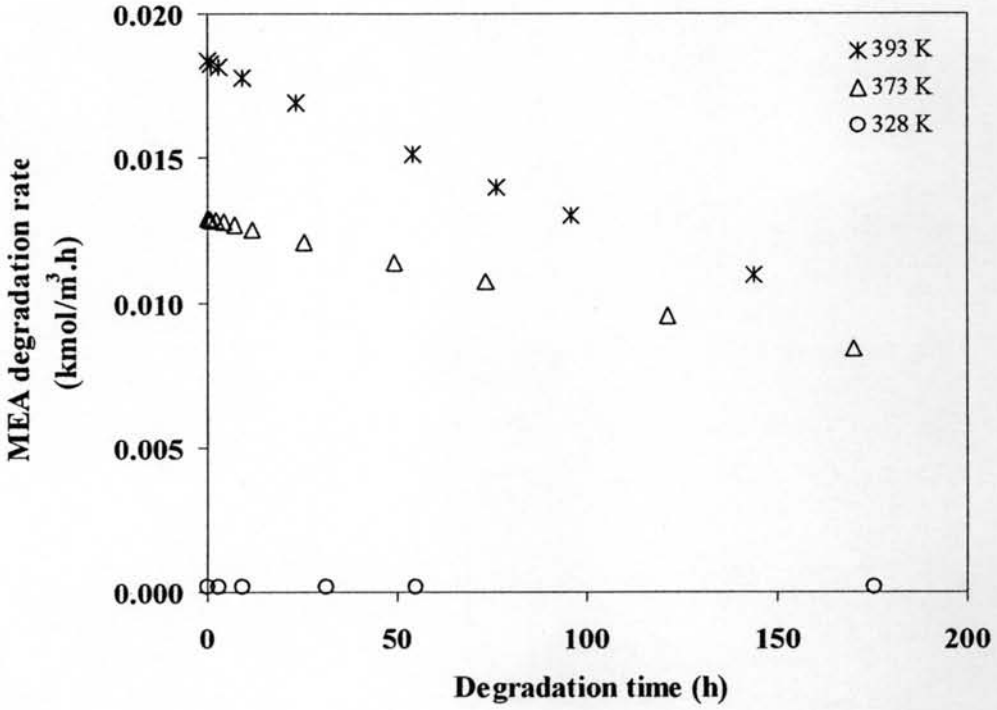

Figure 5.1 Effect of temperature in MEA-O_2 degradation system (5 kmol/m^3 MEA and 100% O_2).

Figure 5.2 also shows that by using 7 kmol/m^3 MEA, 6% O_2, and 11 ppm SO_2, MEA degradation rate was found to be 0.00048 kmol/m^3.h at 373 K. The rate then increased approximately 1.7 times to 0.00018 kmol/m^3.h when the temperature was raised to 393 K.

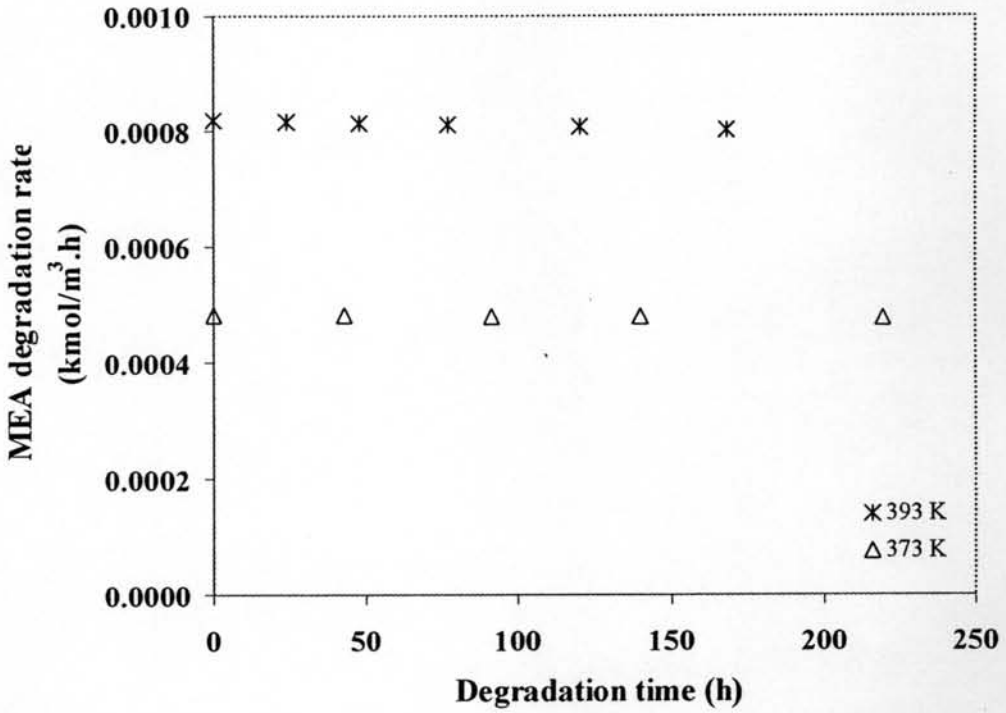

Figure 5.2 Effect of temperature in MEA-O_2-SO_2 degradation system (7 kmol/m^3 MEA, 6% O_2, and 11 ppm SO_2).

Figure 5.3 shows the effect of MEA concentration using the degradation runs with 100% O_2 at a temperature of 393 K. It is clear that an increase in MEA concentration resulted in an increase of the MEA degradation rate.

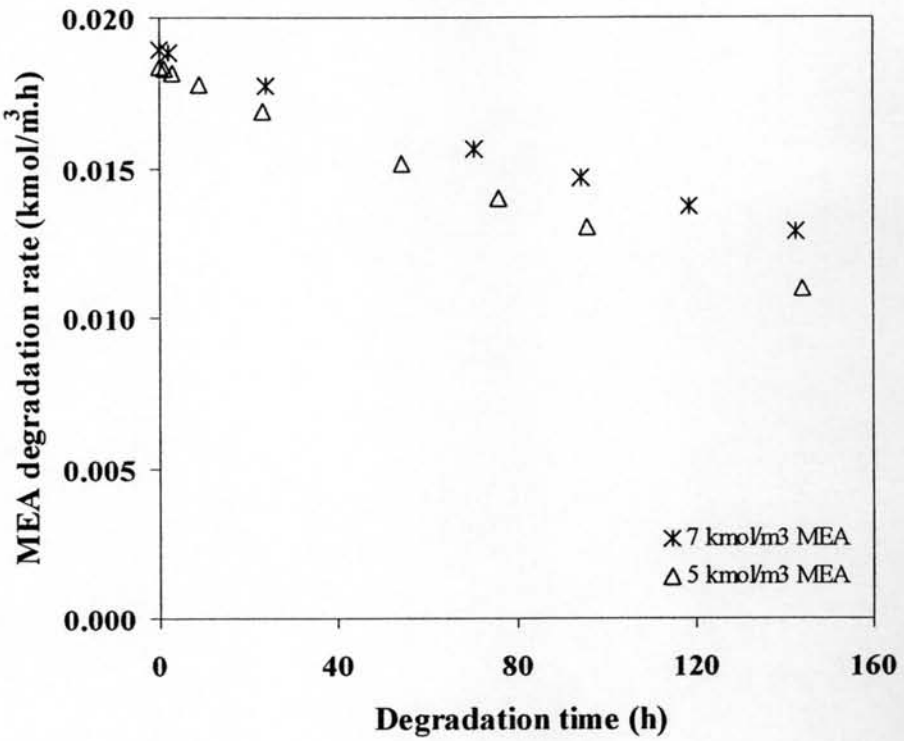

Figure 5.3 Effect of MEA concentration (100% O_2 and 393 K).

Degradation runs involving 6-100% O_2 concentration, 5 kmol/m^3 MEA at 393 K were used to show the effect of O_2 concentration on MEA degradation. A logarithmic scale was used to show this effect as presented in Figure 5.4. This figure shows that an increase in O_2 concentration also results in an increase in the MEA degradation rate.

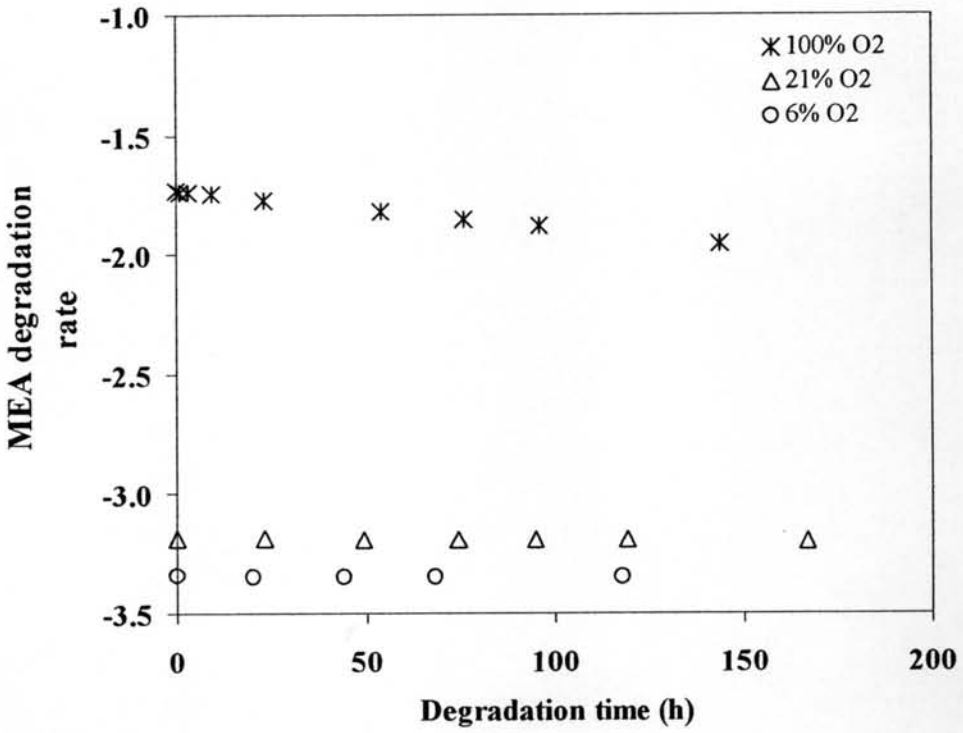

Figure 5.4 Effect O_2 concentration (5 kmol/m^3 MEA and 393 K).

The effect of SO_2 concentration on MEA degradation is demonstrated in Figure 5.5. The runs were conducted at 393 K with 5 kmol/m^3 MEA and 6%O_2 with SO_2 concentration from 0-196 ppm. Figure 5.5 shows that an increase in SO_2 concentration increases the rate of MEA degradation. The two runs conducted at 393 K with 3 kmol/m^3 MEA and somewhat similar values of CO_2 loading (e.g. 0.24 and 0.27 mol CO_2/mol MEA) confirmed the adverse effect of SO_2. The run that contained 196 ppm SO_2 was conducted in the presence of a higher CO_2 loading (0.27 mol CO_2/mol MEA) which is known to retard the degradation rate (Bello and Idem, 2006; Rooney, Dupart, and Bacon, 1998). However, the MEA degradation rate was still higher than that of the run with 11 ppm SO_2 that contained a lower CO_2 loading (0.24 mol CO_2/mol MEA).

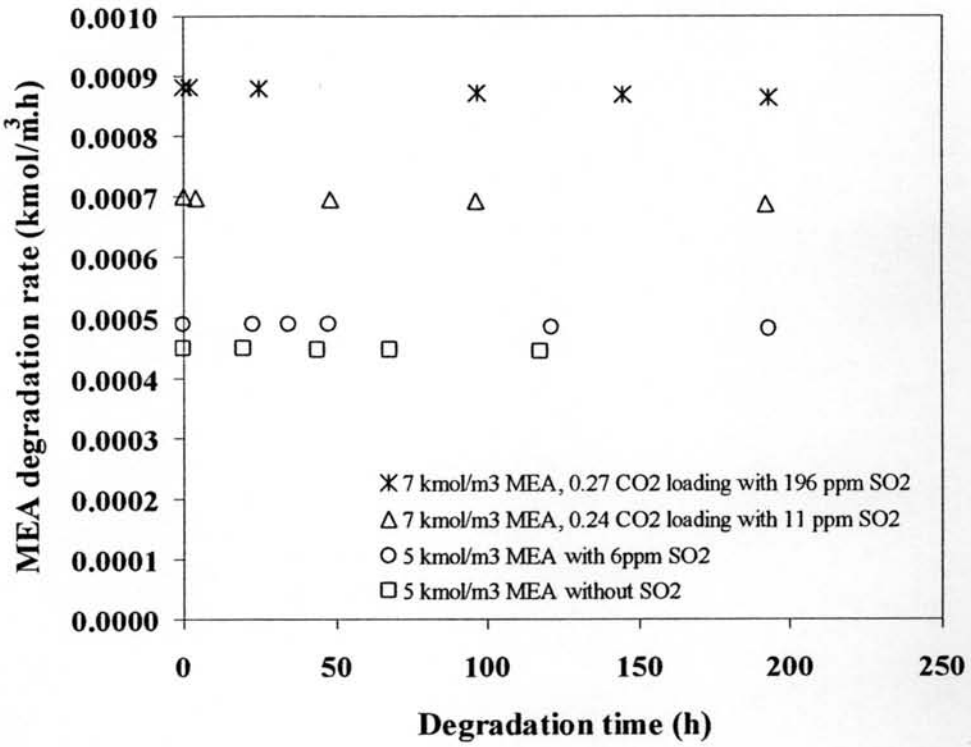

Figure 5.5 Effect of SO_2 concentration (6% O_2 and 393 K).

The effect of CO_2 was also evaluated in this study by varying CO_2 loading values between 0.22-0.52 mole CO_2/mole MEA with 3 kmol/m^3 MEA, 100% O_2 and 373 K. In this study, CO_2 was the only degradation component in which an increase in its concentration resulted in a decrease of the MEA degradation rate. This inhibition effect of CO_2 is shown in Figure 5.6. These results imply that MEA degradation is accelerated by an increase in the concentrations of MEA, O_2 and SO_2, but retarded by an increase in CO_2 loading.

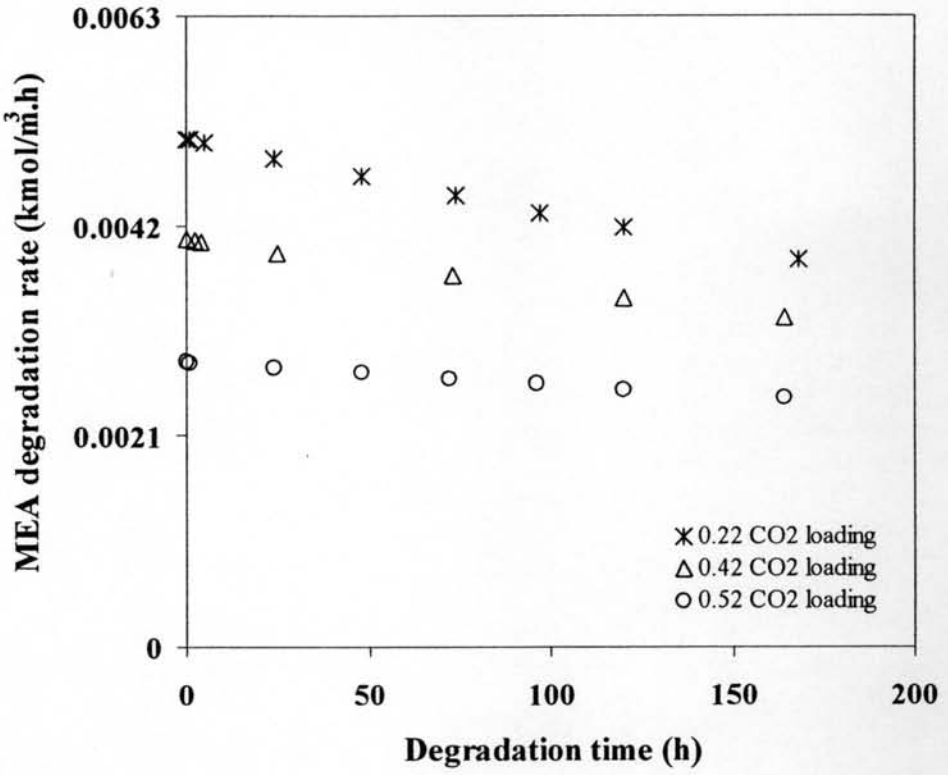

Figure 5.6 Effect of CO_2 concentration (3 kmol/m^3 MEA, 100% O_2, and 373 K).

5.3.2 Estimation of the Parameters of the Kinetic Models

5.3.2.1. Power Law Model

The power law model presented in Equation (5.3) was linearized as given in Equation (5.57) to allow a regression analysis to be performed using a multiple-linear least square technique available in Microsoft Excel 2003 to estimate k_0, E_a, a, b, c and d.

$$\ln(-r_{MEA}) = \ln k_0 - \frac{E_a}{RT} + a\ln[MEA] + b\ln[O_2] + c\ln[SO_2] + d\ln[CO_2] \qquad (5.57)$$

Prior to regression, the values of CO_2 loading were converted to their corresponding concentrations having the same unit as that of MEA

($kmol/m^3$). This was also done for regression of the other models. As well, the O_2 concentration in the MEA solution was obtained using the equation proposed by Rooney and Daniel (1998). This was also used for calculating O_2 concentration for the other models. SO_2 in ppm unit was also converted to $kmol/m^3$ with the assumption that all of the SO_2 in the gas phase was completely dissolved in the liquid phase. This assumption was also used throughout this work. The regression was performed at a 95 % confidence level yielding a coefficient of correlation (R^2) of 0.96. The estimates found for the power law model are tabulated in Table 5.1 for comparison with values of other models. Data of experimental rates, model predicted rates, and %AAD are tabulated in appendix B. A parity plot comparing the experimental and model predicted rates is given in Figure 4.7. The accuracy of the model predictability indicated in terms of percent average absolute deviation (%AAD) was 23%.

5.3.2.2 Modified Power Law Model

Non-linear regression using a non-linear regression software, NLREG version 6.3 (Advanced), was used to estimate the values of the parameters of this kinetic model (Equation (5.4)). The regression was done using all degradation components in $kmol/m^3$ unit as explained in the previous section. The regression estimates were obtained with R^2 of 0.97 and these are also summarized in Table 5.1. Verification of the model was done by a parity plot that compared the experimental with model predicted rates as presented in Figure 5.7. The degradation rate data is given in appendix C. The predictability of the modified power law model was found to be 24% in terms of the AAD.

Table 5.1 Summary of kinetic estimates

Kinetic Model	Power-law based model		Mechanistic-based model	
Parameter	Power law	Modified power law	Split	Combined
Preexponential constant				
k_0	2.41×10^{10}	2.49×10^{9}	-	6.74×10^{9}
k_{01}	-	-	1.65×10^{8}	-
k_{02}	-	-	1.60×10^{-3}	-
Activation energy				
E_a	24,023	29,097	-	29,403
E_{a1}	-	-	16,828	-
E_{a2}	-	-	11,248	-
Degradation order				
MEA				
a	0.13	0.013	0.18	0.015
a'	-	-	0.65	-
O_2				
b	3.27	2.9	2.99	2.91
SO_2				
c	0.07	3.5	2.45	3.52
CO_2				
d	-0.02	-0.03	0.22	0.18
d'	-	-	1.32	-
CO_2 rate constant				
k_1'	-	-	1.13	-
k_2'	-	-	0.00128	1.18
Coefficient of Correlation (R^2)	0.96	0.96	0.98	0.96
Accuracy (%AAD)	23	24	20	25

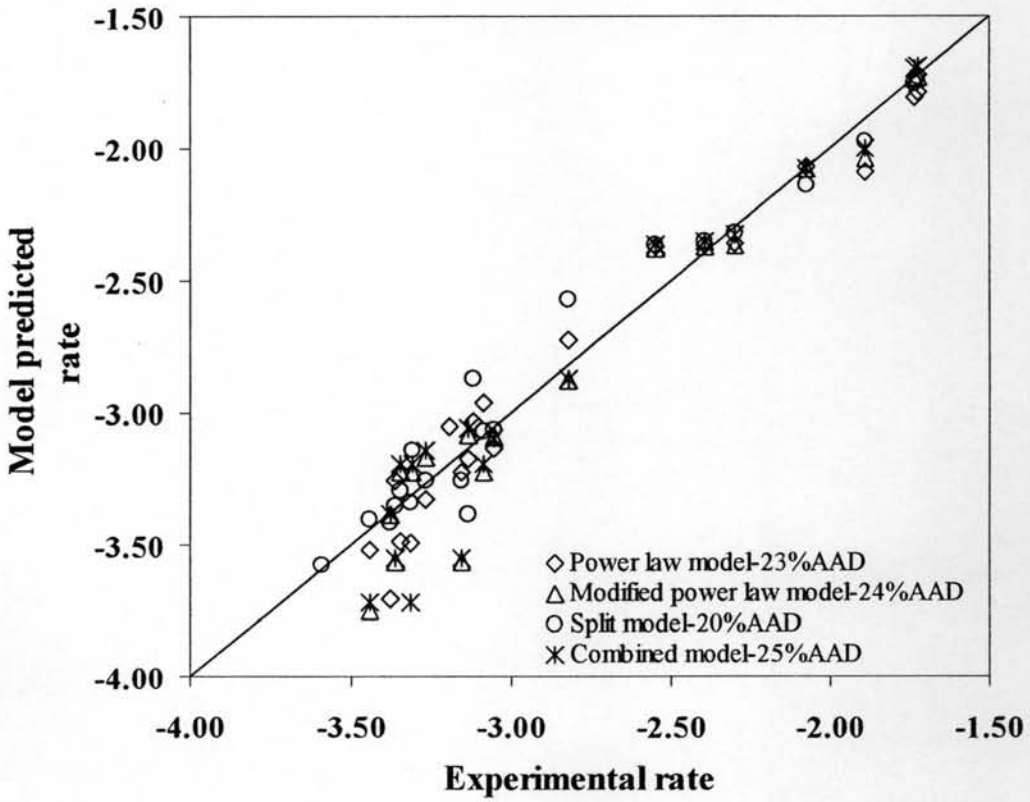

Figure 5.7 Verification and comparison of kinetic models using logarithmic plots of experimental and model predicted rates.

5.3.2.3 Split model

Determination of kinetic parameters for the split model of Equation (5.41) requires more steps than the previous models. As shown in the model, the number of parameters to determine is more than by two the variables that were varied in generating the kinetic data. In order to obtain parameter values which had real physical meaning, the approach was to pre-determine $k_1^{'}$ and $k_2^{'}$ using a combination of appropriate power law equations (e.g. for the system of MEA-O_2-CO_2 and MEA-SO_2-CO_2) and Equations (5.26) and (5.40) previously derived for O_2 and SO_2 pathways, respectively. The pre-determined $k_1^{'}$ and $k_2^{'}$ were subsequently used in Equation (5.41) for final regression to find the rest of the parameters. Since $k_1^{'}$ and $k_2^{'}$ were the most species or temperature independent parameters in Equation (5.41), pre-determining their values during the regression was the appropriate choice.

To determine $k_1^{'}$, a power law-based model was required as given in Equation (5.58).

$$-r_{MEA} = k_{01} e^{\frac{-E_{a1}}{RT}} [MEA]^a [O_2]^b [CO_2]^d \tag{5.58}$$

A multiple-linear regression technique was used to initially obtain k_{01}. The value of k_{01} was later used as k_{01} in Equation (5.26) for further kinetic analysis. Linearization of Equation (5.58) gives Equation (4.59);

$$\ln(-r_{MEA}) = \ln k_{01} - \frac{E_{a1}}{RT} + a \ln[MEA] + b \ln[O_2] + d \ln[CO_2] \tag{5.59}$$

Only experimental runs containing CO_2 as given in were used for regression. The analysis used MEA concentrations between 3 – 7 kmol/m^3, 0.22–0.55 CO_2 loading, 21-100% O_2, and 328 – 393 K degradation temperature. The regression analysis obtained at a 95 % confidence level gave the estimate to be k_{01} as

2.62×10^{11}. The coefficient of correlation (R^2) of 0.98 indicated the accuracy of the value.

The parameter $k_1^{'}$ was estimated using Equation (5.26). To achieve this, the k_{01} value of 2.62×10^{11} obtained earlier from linear regression was substituted as k_{01} in Equation (5.26). The equation was then regressed with non-linear regression software, NLREG, using a new set of data containing 3 – 7 kmol/m^3 MEA, CO_2 loading of 0–0.55 mol CO_2/mol MEA and 6-100% O_2 (both used in kmol/m^3 unit) at degradation temperatures of 328-393 K. The values of $k_1^{'}$ along with E_a, a, b and d obtained from the regression were 1.13, 23762, 0.07, 3.83 and 0.19, respectively. The accuracy of these estimates was indicated by the coefficient of correlation (R^2) of 0.95 and by a parity chart, also in logarithmic scale (19% AAD) as shown in Figure 5.8. Only $k_1^{'}$ determined from the last estimation was used to perform the final regression.

Estimation of $k_2^{'}$ was carried out in the same manner as was done for $k_1^{'}$. Experimental data involved 6%O_2 but various SO_2 concentrations and CO_2 loading values respectively ranging from 6 – 196 ppm and 0.17 – 0.47 mol CO_2/mol MEA were used for linear regression. For this model alone, SO_2 in ppm unit was used throughout the analysis for consistency in magnitudes of the variables. Equation (5.60) was used to first estimate k_{02}.

$$-r_{MEA} = k_{02}e^{\frac{-E_{a2}}{RT}}[MEA]^{a^{'}}[SO_2]^{b}[CO_2]^{d^{'}} \tag{5.60}$$

The regression analysis was carried out at a 95 % confidence level and it resulted in a k_{02} estimate of 0.30 with a coefficient of correlation (R^2) of 0.98. Then, this k_{02} value was substituted as k_{02} into Equation (5.40) and regressed using NLREG software using data including those runs without CO_2. The values of $k_2^{'}$ with E_{a2}, $a^{'}$, b and $d^{'}$ obtained from the final regression were 0.00128, 25668, 0.75, 0.19 and 9.90, respectively. The accuracy of these estimates was indicated by the R^2 of 0.95. Predicted rates calculated using these kinetic estimates were

compared against their corresponding experimental rates to confirm the accuracy of k_2' as shown in Figure 4.8. An AAD of 8% was obtained.

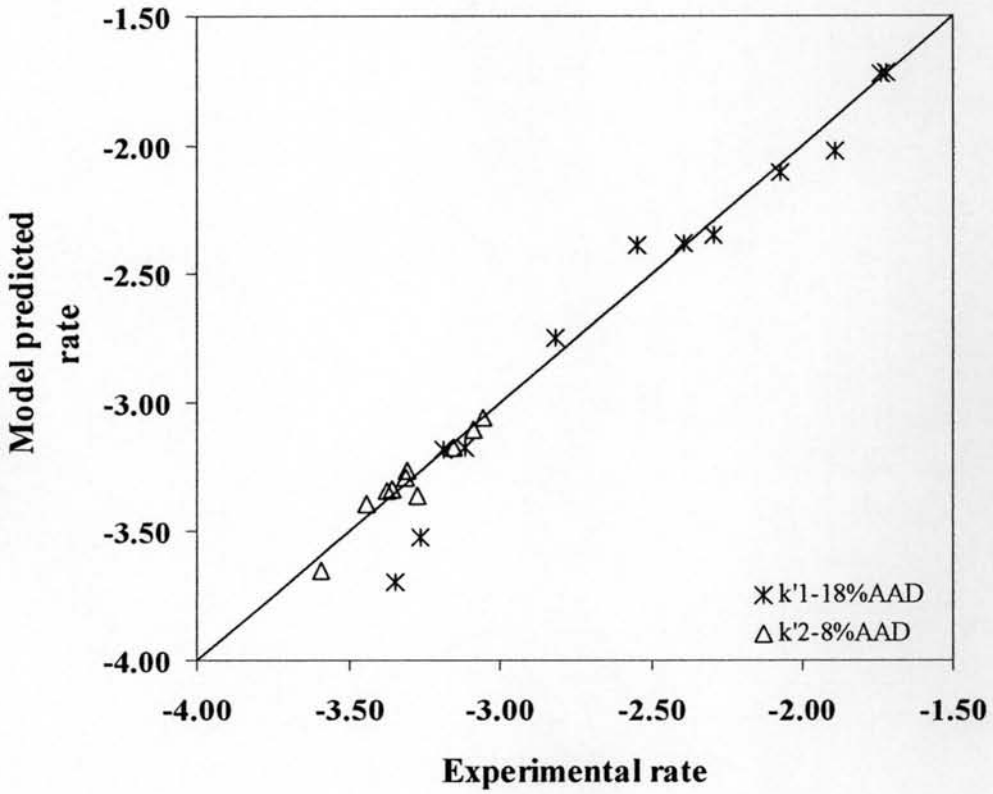

Figure 5.8 Verification of k_1' and k_2' for split model.

To perform the final regression to find the rest of the parameters of the split model, values of $k_1^{'}$ and $k_2^{'}$ found earlier were substituted into Equation (5.41). A non-linear regression was once again performed using data obtained with 3-7 kmol/m^3 MEA, 6-100% O_2, 0-196 ppm SO_2, and loading of 0-0.55 CO_2/mol MEA. The regression estimates obtained with R^2 of 0.98 for k_{01}, E_{a1}, a, b, d, k_{02}, E_{a2}, $a^{'}$, c and $d^{'}$ are also summarized in Table 5.1. A verification of the model also shown in Figure 5.7 was done in the same manner as for the previous models in terms of a parity plot. The rate data is tabulated in appendix D. The model could predict the degradation rate of MEA with approximately 20% AAD.

5.3.2.4 Combined Model

The estimation of the values of the parameters of this model was straightforward. Non-linear regression using NLREG software was required directly for the combined model of Equation (5.56). A similar set of data as used for the split model was regressed with the only exception that SO_2 concentration in kmol/m^3 was used. The non-linear analysis was done at 95% confidence level and the estimates of k_0, E_a, a, b, c, $k_2^{'}$ and d are given in Table 5.1. Once again, verification of the model was carried out in terms of a parity plot of model-based rates versus the experimental rates as shown in Figure 5.7. The rate data is given in appendix E. The model could predict degradation rate of MEA-O_2-SO_2-CO_2 with AAD of 25%.

5.3.3 Analysis of Kinetic Models

The analysis of the models for the degradation of MEA was performed using 3 major criteria involving model limitation in predicting MEA degradation rate, accuracy, and usability in describing the degradation mechanism.

5.3.3.1 Model Limitation in Predicting the Degradation Rate

Although the power law-based model was simple and straightforward, its use was limited to the case in which all degradation components are present. CO_2 absorption from coal-fired flue gas streams is an example of this case. In the case of natural gas flue gas stream, SO_2 may not be present. Also, in the

stripping column section of the CO2 capture plant, O2 may be absent in the liquid phase. Thus, the use of the power law model to predict the degradation rate of MEA during CO_2 removal for these cases would be inappropriate. As well, CO_2 must always be present to make the model valid. Therefore, the model would fail if one wanted to estimate the degradation rate of very lean MEA generated from the regeneration (stripping column) section of the plant. The absence of CO_2 would result in an inappropriate rate of degradation for MEA.

The modified power-law model was developed to overcome the drawback of the power law model. The modification was done so that the model was now applicable in both cases in which O_2 or SO_2 could either be present or absent. Thus, CO_2 capture from flue gas streams of both coal- and natural gas-fired power plants as well as in the absorption section or regeneration section could both benefit from the model in terms of estimating the MEA degradation rate. However, the model was once again, limited to the case in which CO_2 must exist in the system. For split and combined models, their applications were not limited by any of the shortcomings suffered by the power law and the modified power law models. They were both practical for estimating the degradation rate of MEA in CO_2 removal unit from natural gas and flue gas streams either with or without CO_2 in the absorption section or regeneration section of the plant.

5.3.3.2 Model Accuracy

The accuracy of the models developed in this work was also compared in terms of %AAD calculated as the deviations of the experimental rates from the corresponding model predicted rates. The accuracy decreased in the following order; Split model > Power law model > Modified power law model > Combined model. It must be noted that the level of accuracy of these models was however close to each other only ranging between 20-25%. Therefore, it is fair to conclude that as far as the accuracy is concerned, all models could equally estimate the degradation rate of MEA.

5.3.3.3 Model Usability in Describing the Degradation Mechanism

In order to make a kinetic model more meaningful, it must be capable of sufficiently characterizing the degradation mechanism. The empirical

power law and its modified version were only developed without taking into consideration paths taken by MEA, O_2, SO_2 and CO_2 in the degradation process. Thus, none of them was able to satisfactorily mechanistically describe the degradation behaviour of MEA with O_2, SO_2 and CO_2 during the capture process.

On the other hand, the split model derived from a couple of consistent mechanism was capable of giving details of mechanistic behaviour of all the species in the degradation system. It was able to explain in detail the paths taken by MEA and O_2 in one set of mechanism and the paths taken by SO_2 in the other set degrading MEA. A possible drawback was that it still lacked the explanation for a possible interaction of the intermediate products of O_2 and SO_2 induced degrading of MEA which could probably exist during the degradation process.

As discussed, the combined model showed no restriction in predicting the degradation rate of MEA with and without O_2, SO_2 or CO_2, and had an acceptable accuracy as well as the ability in describing the degradation mechanism during the CO_2 removal process. This has made the model the most favourable kinetic equation to represent the degradation system of MEA-O_2-SO_2-CO_2.

5.4 Conclusions

1. Four kinetic models based on power law and mechanism approaches (e.g. power law-based model, modified power law-based model, mechanistic based split model, and mechanistic-based combined model) were developed under the conditions used for CO_2 removal unit to represent MEA degradation as function of temperature and the concentrations of MEA, O_2, SO_2 and CO_2.

2. Based on the limitation, accuracy, and usability in giving mechanistic details, the combined model was favourable to represent MEA degradation in the system involving MEA, O_2, SO_2 and CO_2.